Analysis and Measurements of Nonradiative Dielectric Waveguide Bends

TSUKASA YONEYAMA, SENIOR MEMBER, IEEE, HIDEAKI TAMAKI, AND SHIGEO NISHIDA, SENIOR MEMBER, IEEE

Abstract—**The coupling theory is applied to analyze loss characteristics of the NRD-guide bends. Besides the operating LSM_{01} mode, the parasitic LSE_{01} mode is generated at bends as a result of the mode conversion. A rigorous expression for the coupling coefficient between these two modes is derived and then employed in the two-mode coupling equations to be solved for the bending loss analysis. Design diagrams, which are useful for optimizing the strip width against a given curvature radius to build a lossless bend, are constructed for 90 and 180° NRD-guide bends. It is shown that the field profile at a bend always shifts inwards. This confirms the previous experimental prediction. It is found that the periodic spikes on the loss versus frequency curve of a bend, which have been observed before, can be interpreted as being caused by resonances of the parasitic mode between the transition horns fixed at both ends of the bend, and that the true bending loss itself is normally restricted within a reasonable level.**

As an application of the present theory, a lossless 180° bend with a curvature radius of 5 mm was fabricated with polystyrene and tested at 50 GHz. The measured bending loss was less than 0.3 dB.

I. Introduction

THE nonradiative dielectric waveguide (NRD-guide) consists of dielectric strips which are usually rectangular in cross section and are sandwiched between a below-cutoff parallel plate waveguide. Radiation at curved sections and discontinuities is suppressed due to the below-cutoff nature of the housing, while propagation takes place along the dielectric strips since the cutoff is eliminated because of reduced wavelength in the dielectric. Owing to such a desirable feature, as well as its low-loss property, the NRD-guide is expected to offer a new approach to millimeter-wave integrated circuits. Since the advent of the NRD-guide in 1981 [1], much effort has been devoted to the development of various circuit components [2], [3], but the bends still remain to be studied further.

When transmission was measured of sharp NRD-guide bends whose radii of curvature were two wavelengths or less, periodic spikes were sometimes observed on the loss versus frequency curves (see Fig. 10) [4]. At that time, this phenomenon was qualitatively interpreted as resulting from multiple reflection of waves, which is likely to occur at such sharp bends. Subsequent measurements, however, have revealed that coupling between the operating and the parasitic modes at the curved section is the probable origin of the observed bending loss anomaly.

Manuscript received November 12, 1985; revised March 17, 1986.

T. Yoneyama and H. Tamaki are with the Department of Electronics and Information Engineering, University of the Ryukyus, Nishihara, Okinawa 903-01, Japan.

S. Nishida is with the Research Institute of Electrical Communication, Tohoku University, Sendai 980, Japan.

IEEE Log Number 8609057.

With this in mind, the two-mode coupling theory [5] is applied to analyze loss characteristics of the bends in the NRD-guide. The coupling coefficient, which plays a key role in the analysis, is rigorously calculated by taking into account the metric coefficients of the curved coordinates appropriate to the bend under consideration. It is found that the above-mentioned spikes on the loss curve are caused by resonances of a parasitic mode between the transmitting and receiving horns, and that the true bending loss itself never exceeds a tolerable level, if the bend is properly designed.

By using the design diagrams established here, a lossless 180° bend having a bending radius as small as 5 mm was fabricated and tested at 50 GHz. The measured loss was found to be less than 0.3 dB over the 2 GHz tuning range of an oscillator employed. This is surprising considering the large amount of radiation loss which is encountered in conventional image guide bends [6]. The advantage of the NRD-guide over other dielectric waveguides is obvious since the low-loss compact bends can easily be created.

II. Derivation of Coupled Transmission-Line Equations

Consider a circularly curved NRD-guide bend whose height and width are a and b, respectively, and whose curvature radius is R, as shown in Fig. 1. The height should be less than half a wavelength to assure the NRD-guide operation. The transverse coordinates x and y are taken to be parallel to and perpendicular to the metal plates, respectively, and the longitudinal coordinate z is taken along the mean path of the bend. The metric coefficients for this curved coordinate system are

$$e_1 = 1, e_2 = 1, e_3 = 1 + (x/R). \tag{1}$$

Then, Maxwell's equations are expressed in terms of the transverse field components $\boldsymbol{E}_t$ and $\boldsymbol{H}_t$ as follows:

$$\frac{\partial}{\partial z}\boldsymbol{E}_t = \frac{1}{j\omega\epsilon}\nabla_t e_3 \nabla_t \cdot \boldsymbol{H}_t \times \boldsymbol{i}_z - j\omega\mu e_3 \boldsymbol{H}_t \times \boldsymbol{i}_z \tag{2a}$$

$$\frac{\partial}{\partial z}\boldsymbol{H}_t = \frac{1}{j\omega\mu}\nabla_t e_3 \nabla_t \cdot \boldsymbol{i}_z \times \boldsymbol{E}_t - j\omega\epsilon e_3 \boldsymbol{i}_z \times \boldsymbol{E}_t \tag{2b}$$

where

$$\nabla_t = \boldsymbol{i}_x \frac{\partial}{\partial x} + \boldsymbol{i}_y \frac{\partial}{\partial y} \tag{3}$$

and $\boldsymbol{i}_x, \boldsymbol{i}_y, \boldsymbol{i}_z$ are the unit vectors along the x, y, z coordi-

0018-9480/86/0800-0876$01.00 ©1986 IEEE

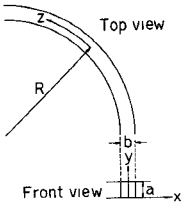

Fig. 1. Front and top views of NRD-guide bend.

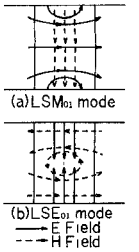

Fig. 2. Rough sketches of field lines in the transverse plane of NRD-guide. (a) For LSM_{01} modes. (b) For LSE_{01} modes.

nate axes, correspondingly. The transverse field components at the bend are assumed to be expanded in the form

$$\boldsymbol{E}_t(x, y, z) = \sum_n V_n(x)\boldsymbol{E}_n(x, y) \tag{4a}$$

$$\boldsymbol{H}_t(x, y, z) = \sum_n I_n(z)\boldsymbol{H}_n(x, y). \tag{4b}$$

In the above equations, $\boldsymbol{E}_n$ and $\boldsymbol{H}_n$ are the transverse field components of the nth mode in the straight NRD-guide with the same cross-sectional dimensions as those of the bend, being so normalized that

$$\int_s \boldsymbol{E}_m \times \boldsymbol{H}_n \cdot \boldsymbol{i}_z \, dS = \begin{cases} 1, & m = n \\ 0, & m \neq n \end{cases} \tag{5}$$

where the integration is carried out over the entire guide cross section S, covering not only the dielectric but also the air regions. The z-dependent coefficients $V_n(z)$ and $I_n(z)$ can be interpreted as the hypothetical voltage and current distributions, respectively, on the equivalent transmission-line corresponding to the nth mode.

Substituting (4) into (2), scalar multiplying (2a) by $\boldsymbol{H}_m \times \boldsymbol{i}_z$ and (2b) by $\boldsymbol{i}_z \times \boldsymbol{E}_m$, and integrating the resulting equations over the whole guide cross section yields

$$\frac{d}{dz} V_m(z) = -j \sum_n X_{mn} I_n(z) \tag{6a}$$

$$\frac{d}{dz} I_m(z) = -j \sum_n B_{mn} V_n(z) \tag{6b}$$

where X_{mn} and B_{mn}, after slight modification, are reduced to

$$X_{mn} = \omega \int_s e_3 (\epsilon E_{zm} E_{zn} + \mu \boldsymbol{H}_m \cdot \boldsymbol{H}_n) \, dS \tag{7a}$$

$$B_{mn} = \omega \int_s e_3 (\mu H_{zm} H_{zn} + \epsilon \boldsymbol{E}_m \cdot \boldsymbol{E}_n) \, dS \tag{7b}$$

E_{zn} and H_{zn} being the longitudinal field components associated with the nth mode in the straight NRD-guide. Equations (6a) and (6b) are the coupled transmission-line equations with the series reactance X_{mn} and the shunt susceptance B_{mn}, which can be calculated once the field expressions for the NRD-guide modes are explicitly determined.

III. Field Expressions for NRD-Guide Modes

The operating mode of the straight NRD-guide is the hybrid LSM_{01} mode with no magnetic field component normal to the air–dielectric interfaces, as shown in Fig. 2(a). The LSM_{01} mode can be viewed as resulting from the lowest TM_0 surface wave mode bouncing back and forth between the parallel metal plates. The first mode number of the NRD-guide mode denotes that of the constituent surface wave mode, while the second one denotes the number of field maxima between the top and bottom plates. Besides the LSM_{01} mode, additional modes need to be considered at a curved section to satisfy the more complicated boundary conditions. Among them, the LSE_{01} mode is most significant since it is nonradiating in nature, and in addition, it has a phase constant closest to that of the operating mode. The closer the phase constants of the relevant modes are, the tighter the coupling between them. The LSE_{01} mode, in contrast to its counterpart, has no electric field component normal to the air–dielectric interfaces, as shown in Fig. 2(b), and can be regarded as being the TE_0 surface wave mode confined between the metal plates. Since it is sufficient to take into account only the LSM_{01} and LSE_{01} modes in the analysis, their normalized field expressions are given below.

For the LSM_{01} mode:

$$E_x = \begin{cases} Ah^2 \sin(\pi y/a)\cos(qx)/\cos(qb/2), \\ \qquad |x| \leq b/2 \\ A\epsilon_r h^2 \sin(\pi y/a)\exp[-p(|x|-b/2)], \\ \qquad |x| \geq b/2 \end{cases} \tag{8a}$$

$$E_y = \begin{cases} -Aq(\pi/a)\cos(\pi y/a)\sin(qx)/\cos(qb/2), \\ \qquad |x| \leq b/2 \\ \mp A\epsilon_r p(\pi/a)\cos(\pi y/a)\exp[-p(|x|-b/2)], \\ \qquad |x| \geq b/2 \end{cases} \tag{8b}$$

$$E_z = \begin{cases} jAq\beta \sin(\pi y/a)\sin(qx)/\cos(qb/2), \\ \qquad |x| \leq b/2 \\ \pm jA\epsilon_r p\beta \sin(\pi y/a)\exp[-p(|x|-b/2)], \\ \qquad |x| \geq b/2 \end{cases} \tag{8c}$$

$$H_x = 0 \tag{8d}$$

$$H_y = \begin{cases} A\omega\epsilon_r\epsilon_0\beta \sin(\pi y/a)\cos(qx)/\cos(qb/2), \\ \qquad |x| \leq b/2 \\ A\omega\epsilon_r\epsilon_0\beta \sin(\pi y/a)\exp[-p(|x|-b/2)], \\ \qquad |x| \geq b/2 \end{cases} \tag{8e}$$

$$H_z = \begin{cases} -jA\omega\epsilon_r\epsilon_0(\pi/a)\cos(\pi y/a)\cos(qx)/\cos(qb/2), \\ \quad |x| \leqslant b/2 \\ -jA\omega\epsilon_r\epsilon_0(\pi/a)\cos(\pi y/a)\exp[-p(|x|-b/2)], \\ \quad |x| \geqslant b/2 \end{cases} \tag{8f}$$

where

$$A = 2q\left\{\omega\epsilon_r\epsilon_0\beta h^2\left[\left(q^2+\epsilon_r^2p^2\right) + 2\epsilon_r(\epsilon_r-1)k_0^2/pb\right]ab\right\}^{-1/2}. \tag{9}$$

For the LSE_{01} mode:

$$E_x = 0 \tag{10a}$$

$$E_y = \begin{cases} -\hat{A}\omega\mu_0\hat{\beta}\cos(\pi y/a)\cos(\hat{q}x)/\cos(\hat{q}b/2), \\ \quad |x| \leqslant b/2 \\ -\hat{A}\omega\mu_0\hat{\beta}\cos(\pi y/a)\exp[-\hat{p}(|x|-b/2)], \\ \quad |x| \geqslant b/2 \end{cases} \tag{10b}$$

$$E_z = \begin{cases} -j\hat{A}\omega\mu_0(\pi/a)\sin(\pi y/a)\cos(\hat{q}x)/\cos(\hat{q}b/2), \\ \quad |x| \leqslant b/2 \\ -j\hat{A}\omega\mu_0(\pi/a)\sin(\pi y/a)\exp[-\hat{p}(|x|-b/2)], \\ \quad |x| \geqslant b/2 \end{cases} \tag{10c}$$

$$H_x = \begin{cases} \hat{A}\hat{h}^2\cos(\pi y/a)\cos(\hat{q}x)/\cos(\hat{q}b/2), \\ \quad |x| \leqslant b/2 \\ \hat{A}\hat{h}^2\cos(\pi y/a)\exp[-\hat{p}(|x|-b/2)], \\ \quad |x| \geqslant b/2 \end{cases} \tag{10d}$$

$$H_y = \begin{cases} \hat{A}\hat{q}(\pi/a)\sin(\pi y/a)\sin(\hat{q}x)/\cos(\hat{q}b/2), \\ \quad |x| \leqslant b/2 \\ \pm\hat{A}\hat{p}(\pi/a)\sin(\pi y/a)\exp[-\hat{p}(|x|-b/2)], \\ \quad |x| \geqslant b/2 \end{cases} \tag{10e}$$

$$H_z = \begin{cases} j\hat{A}\hat{q}\hat{\beta}\cos(\pi y/a)\sin(\hat{q}x)/\cos(\hat{q}b/2), \\ \quad |x| \leqslant b/2 \\ \pm j\hat{A}\hat{p}\hat{\beta}\cos(\pi y/a)\exp[-\hat{p}(|x|-b/2)], \\ \quad |x| \geqslant b/2 \end{cases} \tag{10f}$$

where

$$\hat{A} = 2\hat{q}\left\{\omega\mu_0\hat{\beta}\hat{h}^2(\epsilon_r-1)k_0^2(1+2/\hat{p}b)ab\right\}^{-1/2}. \tag{11}$$

In the above equations, ϵ_0, μ_0, and k_0 are the permittivity, permeability, and wavenumber of the free space, ϵ_r is the relative dielectric constant of the strip, and the upper and lower signs apply to the air regions defined by $x > b/2$ and $x < -b/2$, respectively. Other parameters are related by

$$h^2 = \epsilon_r k_0^2 - q^2 = k_0^2 + p^2 \tag{12a}$$

$$h^2 = \epsilon_r k_0^2 - \hat{q}^2 = k_0^2 + \hat{p}^2 \tag{12b}$$

$$\beta = \sqrt{h^2 - (\pi/a)^2} \tag{13a}$$

$$\hat{\beta} = \sqrt{\hat{h}^2 - (\pi/a)^2} \tag{13b}$$

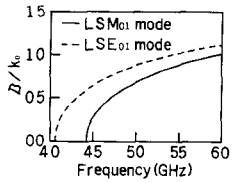

Fig. 3. Normalized phase constants of LSM_{01} and LSE_{01} modes as a function of frequency for a polystyrene strip 2.7 mm in height and 2.4 mm in width.

where q, p, $\hat{q}$, and $\hat{p}$ are the first eigenvalues of the following characteristic equations, respectively:

$$q\tan(qb/2) = \epsilon_r p, \qquad q^2 + p^2 = (\epsilon_r - 1)k_0^2 \tag{14a}$$

$$\hat{q}\tan(\hat{q}b/2) = \hat{p}, \qquad \hat{q}^2 + \hat{p}^2 = (\epsilon_r - 1)k_0^2. \tag{14b}$$

Physically speaking, h and $\hat{h}$ are the phase constants of the lowest TM_0 and TE_0 surface wave modes supported by a dielectric slab with a thickness of b, while β and $\hat{\beta}$ are the phase constants of the LSM_{01} and LSE_{01} NRD-guide modes, respectively. For reference, the phase constants β and $\hat{\beta}$ are shown in Fig. 3 as a function of frequency for a typical polystyrene NRD-guide ($\epsilon_r = 2.56$) 2.7 mm in height and 2.4 mm in width. Since the parasitic LSE_{01} mode has a lower cutoff frequency than the LSM_{01} mode and is, moreover, nonradiating, it is difficult to suppress the LSE_{01} mode once generated in the guide.

IV. Solution of Coupling Equations

Coupling between the LSM_{01} and LSE_{01} modes is dominant at bends, and hence only these two modes are considered in the analysis. Therefore, the mode numbers for the LSM_{01} and LSE_{01} modes are simply denoted by 1 and 2, respectively. Then, (6) is reduced to

$$\frac{dV_1}{dz} = -jX_{11}I_1 - jX_{12}I_2 \tag{15a}$$

$$\frac{dI_1}{dz} = -jB_{11}V_1 - jB_{12}V_2 \tag{15b}$$

$$\frac{dV_2}{dz} = -jX_{21}I_1 - jX_{22}I_2 \tag{15c}$$

$$\frac{dI_2}{dz} = -jB_{21}V_1 - jB_{22}V_2. \tag{15d}$$

Each equivalent transmission-line parameter can be calculated by substituting the field expressions (8) and (10) into (7) as follows:

$$X_{11} = B_{11} = \beta \tag{16a}$$

$$X_{22} = B_{22} = \hat{\beta} \tag{16b}$$

$$X_{12} = X_{21} = \pi\epsilon_r(\epsilon_r - 1)A\hat{A}k_0^2\beta p/\left[(q^2 - \hat{q}^2)R\right] \tag{16c}$$

$$B_{12} = B_{21} = \pi\epsilon_r(\epsilon_r - 1)A\hat{A}k_0^2\hat{\beta}p/\left[(q^2 - \hat{q}^2)R\right]. \tag{16d}$$

At this stage of analysis, it is convenient to introduce the complex amplitude coefficients a_n and b_n for the forward and backward traveling waves, respectively. Since the mode impedances are 1 Ω for all modes in the present scheme of field normalization [see (5)], the complex amplitude coeffi-

cients are simply expressed in the form

$$a_n = (V_n + I_n)/2, \qquad n = 1,2 \tag{17a}$$

$$b_n = (V_n - I_n)/2, \qquad n = 1,2. \tag{17b}$$

Applying (17) to (15) yields

$$\frac{da_1}{dz} = -j\frac{1}{2}(X_{11} + B_{11})a_1 - j\frac{1}{2}(X_{12} + B_{12})a_2 \tag{18a}$$

$$\frac{da_2}{dz} = -j\frac{1}{2}(X_{21} + B_{21})a_1 - j\frac{1}{2}(X_{22} + B_{22})a_2. \tag{18b}$$

In deriving the above equations, the backward waves are ignored because of their very weak coupling effect.

The coefficients for a_1 in (18a) and for a_2 in (18b) can be interpreted as the phase constants of the LSM_{01} and LSE_{01} modes at the bend, and by means of (16) they are written as

$$(X_{11} + B_{11})/2 = \beta, \qquad \text{for } LSM_{01} \text{ mode,} \tag{19a}$$

$$(X_{22} + B_{22})/2 = \hat{\beta}, \qquad \text{for } LSE_{01} \text{ mode,} \tag{19b}$$

indicating that the curvature of the guide has no effect at all on the phase constants. The other two coefficients in (18), which are actually identical, are the coupling coefficients between the relevant two modes, and become

$$c = (X_{12} + B_{12})/2 = (X_{21} + B_{21})/2$$
$$= \pi\epsilon_r(\epsilon_r - 1)A\hat{A}k_0^2 p(\beta + \hat{\beta})/[2(q^2 - \hat{q}^2)R]. \tag{20}$$

Substituting (9) and (11) into the above expression leads to

$$c = 2\pi \frac{\sqrt{\epsilon_r(\epsilon_r - 1)}}{h\hat{h}ab} \frac{q\hat{q}}{(q^2 - \hat{q}^2)R} \times \frac{P\left(\sqrt{\beta/\hat{\beta}} + \sqrt{\hat{\beta}/\beta}\right)}{\left\{\left[(q^2 + \epsilon_r^2 p^2) + 2\epsilon_r(\epsilon_r - 1)k_0^2/pb\right](1 + 2/pb)\right\}^{1/2}} \tag{21}$$

By using (19) and (20), (18) is reduced to the well-known coupling equations [5]

$$\frac{da_1}{dz} = -j\beta a_1 - jca_2 \tag{22a}$$

$$\frac{da_2}{dz} = -jca_1 - j\hat{\beta}a_2. \tag{22b}$$

Solving them under the initial conditions

$$a_1(0) = 1, \qquad a_2(0) = 0 \tag{23}$$

yields

$$a_1(z) = \exp(-j\beta_0 z)[\cos(\Gamma z/2) - j(\Delta\beta/\Gamma)\sin(\Gamma z/2)] \tag{24a}$$

$$a_2(z) = -j(zc/\Gamma)\exp(-j\beta_0 z)\sin(\Gamma z/2) \tag{24b}$$

where

$$\beta_0 = (\beta + \hat{\beta})/2 \tag{25a}$$

$$\Delta\beta = \beta - \hat{\beta} \tag{25b}$$

$$\Gamma = \sqrt{\Delta\beta^2 + 4c^2}. \tag{25c}$$

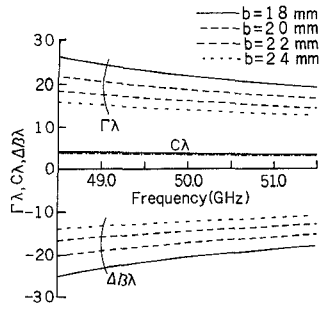

Fig. 4. Parameters c, $\Delta\beta$, and Γ as a function of frequency for polystyrene NRD-guide bends 16 mm in radius of curvature, 2.7 mm in height, and having different widths.

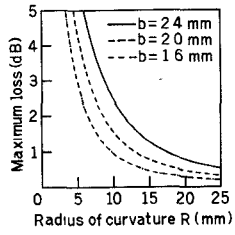

Fig. 5. Maximum bending loss as a function of bending radius at 50 GHz for polystyrene strips 2.7 mm in height and having different widths.

In particular, the amplitude of the operating mode is

$$|a_1(z)| = \left[|-(4c^2/\Gamma^2)\sin^2(\Gamma z/2)\right]^{1/2} \tag{26}$$

and hence the bending loss is given by

$$L = -10\log\left[1 - (4c^2/\Gamma^2)\sin^2(\Gamma z/2)\right] \quad \text{(dB)}. \tag{27}$$

Accordingly, the maximum bending loss becomes

$$L_{\max} = 20\log(\Gamma/\Delta\beta) \quad \text{(dB)}. \tag{28}$$

V. Results and Discussions

Polystyrene ($\epsilon_r = 2.56$) strips 2.7 mm in height, but having different widths, are assumed throughout the paper for carrying out numerical computation at a center frequency of 50 GHz. Since the bending loss is a function of the parameters c, $\Delta\beta$, and Γ, they are plotted versus frequency for a curvature radius of 16 mm in Fig. 4. It is interesting to note that the phase constant difference $\Delta\beta$ changes its magnitude as the strip width varies, but the magnitude change of the coupling coefficient c is only slight.

The maximum bending loss is shown as a function of the bending radius for different strip widths in Fig. 5. The loss not only decreases with an increasing bending radius as expected, but also decreases with a decreasing dielectric strip width. This is due to an increase in the phase constant difference between the two modes, as can be seen in Fig. 4.

The maximum bending loss is a convenient measure for the upper bound of possible loss, but it often leads to an overestimation. Actually, the bending loss can even be eliminated if the dielectric strip width is optimized for a given curvature radius of the bend at a specified frequency. This can be shown by putting $z = \pi R/2$ and $z = \pi R$ in

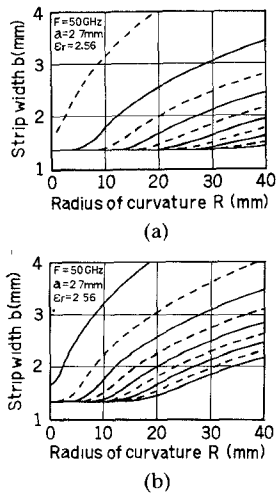

Fig. 6. Design diagrams for polystyrene NRD-guide bends 2.7 mm in height at 50 GHz. (a) 90°. (b) 180°. Solid and dotted curves correspond to the lossless and maximum loss bends, respectively.

(27) to obtain expressions for the bending loss of 90 and 180° bends, respectively. Then it is easy to find that the bending loss of the 90° bend vanishes when

$$\Gamma R = 4n, \qquad n = 1,2,\cdots \tag{29a}$$

and is maximized when

$$\Gamma R = 4n-2, \qquad n = 1,2,\cdots. \tag{29b}$$

Similar equations for the 180° bend become

$$\Gamma R = 2n, \qquad n = 1,2,\cdots \tag{30a}$$

$$\Gamma R = 2n-1, \qquad n = 2,3,\cdots \tag{30b}$$

correspondingly. The case of $n=1$ should be excluded from (30b) since $\Gamma R > 1$ always holds. Equations (29) and (30) are plotted in the bending radius versus strip width relation in Fig. 6(a) and (b). The solid curves correspond to the lossless bend, while the dotted ones correspond to the maximum loss bend. Comparison between Fig. 6(a) and (b) shows that the bending radius of a lossless 180° bend can be half of that of the lossless 90° bend with the same strip width. This is due to the fact that a lossless 180° bend can be created by connecting not only two lossless 90° bends but also two maximum-loss 90° bends in series since the parasitic LSE_{01} mode built up at its maximum in the first half of the 180° bend is completely coupled back to the LSM_{01} mode during a trip in the latter half. The diagrams are especially useful for designing bends of minimum loss. A 180° bend, for instance, will be lossless if a strip width of 2.5 mm is chosen for a curvature radius of 5 mm, as Fig. 6(b) indicates. A 90° bend with a strip width of 2.5 mm and a curvature radius of 10 mm will also be lossless, as can be seen in Fig. 6(a). Loss measurement of these two bends connected in tandem will be described in Section VII.

Fig. 6 reveals that the bending loss varies, taking maximum and minimum values as a function of the strip width for a fixed bending radius. This is shown for the 90° bends in Fig. 7. The bending loss undulates at first and then increases monotonously as the strip width increases. This

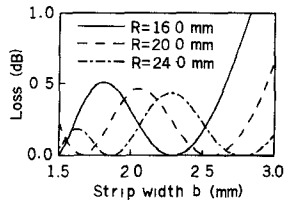

Fig. 7. Bending loss of the 90° polystyrene NRD-guide bend at 50 GHz as a function of the strip width for various radii of curvature.

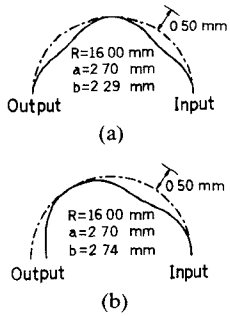

Fig. 8. Trajectories of the field maximum in 180° polystyrene NRD-guide bends 16 mm in bending radius. (a) 2.29 mm in strip width. (b) 2.74 mm in strip width.

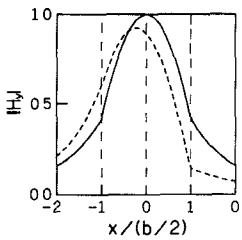

Fig. 9. Field profiles at positions of maximum (dotted curve) and no (solid curve) field shifts for the 180° polystyrene NRD-guide bend 2.29 mm in width and 16 mm in bending radius.

is also the case for the 180° bends. This fact suggests that modification should be made of the previous experimental conclusion which stated that a decrease in strip width is effective for reducing bending loss [4]. That statement is valid only for large strip widths in light of Fig. 7.

Since the fields at a curved section are a mixture of the symmetrical LSM_{01} and asymmetrical LSE_{01} fields, the field maximum follows a winding path as waves propagate in the guide. Typical trajectories of the field maximum are shown in Fig. 8 for two particular 180° bends, one with a strip width of 2.29 mm and the other with a strip width of 2.74 mm. For visual convenience, the trajectories are magnified ten times in the transverse direction. Shown in Fig. 8(a) is the lossless case where the field maximum coincides with the center of the strip at exit, while shown in Fig. 8(b) is the maximum-loss case where the transverse field shift becomes maximum at exit. The inward shift of the field maximum is peculiar to the NRD-guide bend, as pointed out in a previous paper [4]. For reference, the profiles of the field component H_y are calculated at positions where maximum and no field shift are to occur, and are compared in Fig. 9. The field profile without shift is, of course, the same as that in the straight guide, while the shifted one is highly nonsymmetrical.

VI. Effects of Transition Horns on Loss Characteristics

The spikes on the loss versus frequency curves of the sharp bends, which have been observed before [4], cannot be interpreted in terms of the present theory alone unless reflection by the transition horns is considered. The transition horns used in measurement are so designed that only the operating LSM_{01} mode is matched to the metal waveguide with return loss higher than 24 dB [2], but the cross-polarized LSE_{01} mode is almost reflected back. Thus, the LSE_{01} mode, once generated at bend, exhibits resonance behavior between the transmitting and receiving transition horns at certain discrete frequencies. By taking such an effect of resonance into consideration, the amplitude of the operating mode at the receiving horn can be calculated to be

$$|a_m| = |a_1(l_0) + r'a_2^2(l_0) \sum_{n=1}^{\infty} [r'\hat{a}_1(l_0)]^{2n-1}|$$

$$= \left| \frac{1-\exp(-j\phi)r^2}{1-\exp(-j\phi)r^2|a_1|^2} a_1 \right| \tag{31}$$

where

$$\phi = 2\beta_0 l_0 + 2\hat{\beta}(l_1+l_2) - 2\tan^{-1}[(\Delta\beta/\Gamma)\tan(\Gamma l_0/2)] \tag{32a}$$

$$r' = \exp[-j\hat{\beta}(l_1+l_2)]r. \tag{32b}$$

In the above expressions, r is the reflection coefficient of the transition horn, l_0 is the mean path length of the bend, l_1 and l_2 are distances from the ends of the bend to the throats of the transmitting and receiving horns, respectively, where the LSE_{01} wave is reflected back, and $\hat{a}_1(l_0)$ is given by (24a) with $\Delta\beta$ changed in sign. Physically, the leading term in the first equation of (31) represents the main contribution due to the first passage of a wave through the bend, while each term under the summation represents the perturbation which is caused by successive processes of the LSM_{01}-to-LSE_{01} mode conversion, multiple reflection by the horns, and the reverse LSE_{01}-to-LSM_{01} mode conversion.

Assuming that $l_1 = l_2 = 5$ cm, $r = 0.85$, the curvature radius of the bend is 16 mm, and the strip width is 2.6 mm, the loss of the 180° bend is calculated as a function of frequency and compared with measured data in Fig. 10. Since the assumed bend is rather lossy, the spikes are notable. Agreement between the calculated and measured values is excellent, and hence the present explanation for the observed bending loss characteristics may be acceptable. The dotted curve in Fig. 10(a) shows the theoretical bending loss of the same bend, but with the parasitic mode resonance ignored. This is the true bending loss and is considerably smaller than the peak values in magnitude. Since all NRD-guide components, including oscillators and detectors, are to be assembled between a below-cutoff parallel plate waveguide at the final stage of development, no transition horns are needed. In such cases, sharp bends can be incorporated into integrated circuits without causing any serious trouble to performance over a sufficient bandwidth at millimeter wavelengths.

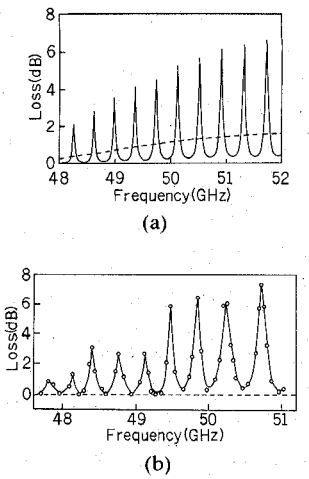

Fig. 10. (a) Calculated and (b) measured bending loss of a 180° polystyrene NRD-guide bend 2.7 mm in height, 2.6 mm in width, and 16 mm in radius of curvature. Reflection of the LSE_{01} mode by the transition horns is taken into account in calculation. Dotted curve in (a) is calculated by ignoring the reflection by the transition horns.

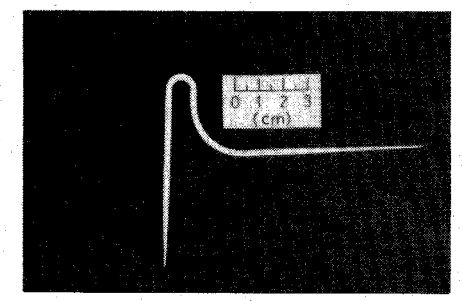

Fig. 11. Fabricated bending structure consisting of lossless 180 and 90° polystyrene NRD-guide bends connected in series. The 180 and 90° bends are 5 and 10 mm in radius of curvature, respectively.

VII. Measurements of Bending Losses

For another confirmation of the theory, lossless bends were designed, fabricated with polystyrene, and measured at 50 GHz. A photograph of the fabricated bending structure, which consists of 90 and 180° bends connected in series, is shown in Fig. 11. The curvature radius of the 90° bend is 10 mm, and that of the 180° bend is as small as 5 mm. The optimum dielectric strip width was determined to be 2.5 mm for both the bends by referring to Fig. 6. The 90° bend was incorporated to avoid mechanical as well as electrical interference between the transmitting and receiving horns which would occur with the 180° bend alone.

Bending losses were measured by comparing transmissions of the compound bend and a straight strip equal in length. The obtained data are shown in Fig. 12 over the frequency range from 49 to 51 GHz of a manual tuning klystron oscillator. The overall bending loss was found to be less than 0.3 dB. This residual loss may be in part due to the avoidable measurement error and in part due to the nontrivial reflection at such sharp bends. The periodic spikes as depicted in Fig. 10 never appeared on the loss versus frequency curve in the present measurement. The

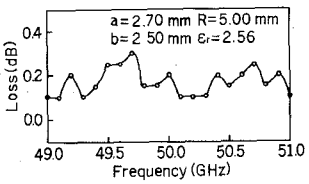

Fig. 12. Measured bending loss of the compound bending structure consisting of 180 and 90° bends connected in series, as shown in Fig. 11.

results clearly show the advantage of the NRD-guide over other dielectric waveguides, which suffer from a large amount of radiation loss at bends [6].

VIII. Conclusions

The NRD-guide bend is analyzed by means of the coupling theory. It is found that the bending loss can be minimized if the strip width is optimized for a given curvature radius of the bend at a specified frequency. The periodic spikes on the loss versus frequency curve of the bend can be interpreted in terms of resonance of the parasitic LSE_{01} mode between the transition horns. When transition horns are not needed, as would be the case in the final stage of the development of the NRD-guide-based integrated circuits, the bending loss is expected to be considerably smaller than the observed loss peaks, and hence does not cause any serious trouble to circuit performance. A very sharp 180° bend with a curvature radius of 5 mm was fabricated at 50 GHz, and its bending loss was found to be less than 0.3 dB at most. This clearly demonstrates the advantage of the NRD-guide over other dielectric waveguides, which suffer from a large amount of radiation loss at bends.

References

[1] T. Yoneyama and S. Nishida, "Nonradiative dielectric waveguide for millimeter-wave integrated circuits," *IEEE Trans. Microwave Theory Tech.*, vol. MTT-29, pp. 1188–1192, Nov. 1981.

[2] T. Yoneyama, "Nonradiative dielectric waveguide," in *Infrared and Millimeter-Waves*, Vol. 11, K. J. Button, Ed. New York: Academic Press, 1984, pp. 61–98.

[3] T. Yoneyama, F. Kuroki, and S. Nishida, "Design of nonradiative dielectric waveguide filters," *IEEE Trans. Microwave Theory Tech.*, vol. MTT-32, pp. 1659–1662, Dec. 1984.

[4] T. Yoneyama, M. Yamaguchi, and S. Nishida, "Bends in nonradiative dielectric waveguides," *IEEE Trans. Microwave Theory Tech.*, vol. MTT-30, pp. 2146–2150, Dec. 1982.

[5] S. P. Morgon, "Theory of curved circular waveguide containing an inhomogeneous dielectric," *Bell Syst. Tech. J.*, vol. 36, pp. 1209–1251, Sept. 1957.

[6] K. Solbach, "The measurement of the radiation losses in dielectric image line bends and the calculation of a minimum acceptable curvature radius," *IEEE Trans. Microwave Theory Tech.*, vol. MTT-27, pp. 51–53, Jan. 1979.

Tsukasa Yoneyama (S'60–M'64–SM'84) graduated from Tohoku University, Sendai, Japan, in 1959 and received the M.E. and Ph.D. degrees in electrical communication engineering from Tohoku University in 1961 and 1964, respectively.

From 1964 to 1983 he was an Associate Professor at the Research Institute of Electrical Communication, Tohoku University. In April 1983 he joined the University of the Ryukyus, Okinawa, Japan, where he is now a Professor in the Department of Electronics and Information Engineering. His research interests are concerned with electromagnetic field theory and millimeter-wave integrated circuits.

Dr. Yoneyama is a member of the IECE of Japan.

✠

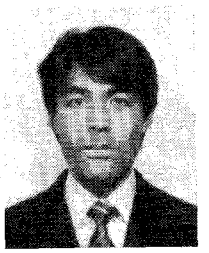

Hideaki Tamaki was born in Okinawa, Japan, on December 1, 1962. He received the B.E. degree in electrical engineering from the University of the Ryukyus, Okinawa, in 1985.

In April 1985 he joined the Research and Development division at Graphica Computer Corporation where he is now working on the design of image processors.

✠

Shiegeo Nishida (SM'59) was born in Nagoya, Japan, on March 7, 1924. He graduated from Tohoku University, Sendai, Japan, in 1949 and received the Ph.D. degree from Tohoku University in 1959.

He was appointed a Research Associate and an Associate Professor at the Research Institute of Electrical Communication, Tohoku University, in 1949 and 1955, respectively. From 1957 to 1959, on leave of absence from Tohoku University, he joined the Microwave Research Institute of the Polytechnic Institute of Brooklyn, Brooklyn, NY, where he was engaged in the research on microwave waveguides and antennas. Since 1964 he has been a Professor at Tohoku University, and his major interests are in microwave and optical-wave transmissions.